# Factors influencing vibrations in a magnetically suspended pump

Yichen Yao [a,b], Yanhui Ma [a], Yixin Su [a], Suyuan Yu [a,#]

[a] Department of Energy and Power Engineering, Tsinghua University, Beijing 100084, China
[b] School of Energy and Environment, Southeast University, Nanjing, 210096, China
[#] Corresponding author Email: suyuan@mail.tsinghua.edu.cn

***Abstract*—Vibrations are a common problem in pumps that reduce the pump efficiency, cause excessive noise, and can even induce fatigue failures. Active magnetic bearings (AMBs) have been extensively investigated to reduce vibrations. Most research has focused on control methods to reduce the vibrations, but the mechanical characteristics of the bearing are also important for vibration isolation since they are the main vibration transfer path. A finite element model of a 30 kW pump prototype suspended on 5-DOF AMBs was used to analyze the pump vibrations with the AMBs simplified to spring-dampers with equivalent stiffness and the damping related to the rotational speed. Two external excitations were analyzed with an unbalanced centrifugal force acting on the rotor in one case and the other case having a hydrodynamic force acting on the impeller. The model was simplified to improve the simulation efficiency by using a time dependent hydrodynamic force obtained from a CFD model that was assumed to not be affected by the system parameter changes. The model was then used to investigate the effects of several key structural parameters on the magnetic pump vibrations, including the motor shell thickness, the junction box position, the stiffness and damping of the magnetic bearing and the isolator as well as the mounting method. Then, the results were used to design a new pump with FE simulations used to judge the effectiveness of the design. The simulations show that the design effectively suppresses the vibrations at the working speed. This research provides a method for designing pumps with less vibrations.**

## I. INTRODUCTION

Rotating machinery is frequently used as power equipment in industry, including fans, pumps, motors, steam turbines, and jet engines. However, vibration and noise in the rotating machinery not only seriously affects the machine service life, but also pollutes the environment and can harm the physical and mental health of the operators[1]. The two main sources of vibrations in rotating machinery are the centrifugal force caused by asymmetric structures, materials and assembly errors and the external excitement caused by electromagnetic forces and the flow. The vibration generated in the machine are transferred to the machine base through the support structure and then to the outside world. Increasing speeds and powers are making the problem of vibration suppression in rotating machinery more and more difficult. Unlike traditional mechanical bearings, magnetic levitation bearings have no mechanical wear, no contact and can work at very high speeds, which are ideal characteristics for supporting rotating machinery. They are also particularly suitable for providing active control of rotor vibrations [2].

Generally speaking, AMBs reduce vibrations in three ways. AMB's improve self-balancing of the rotor by reducing or eliminating rotor imbalances [3]. Secondly, the AMB controller can be optimized for the external excitation forces on the rotating machinery to actively reduce the vibrations [4]. Thirdly, the control parameters can be adjusted to change the bearing stiffness and damping to improve the vibration transmission characteristics of the rotating machinery and reduce vibration transmission through the system [5].

In recent years, many studies have focused on designing AMBs to suppress vibrations in rotating machinery. Tanaka et al. [6] proposed a new modeling method called the Extended Reduced Order Physical Modeling Method which describes a continuous system based on the vibration modes to design an AMB controller to rotate a flywheel rotor while passing through critical speeds caused by flexible modes. Zheng and Feng [7] proposed a feedforward control strategy combined with an adaptive notch filter to resolve rotor imbalance problems in magnetically suspended centrifugal compressors. The adaptive notch filter identified imbalance signals due to displacements and produced a compensation signal to eliminate the unbalanced current components. The controller also produced a feed-forward control signal with an inverse power amplifier to compensate for the negative displacement stiffness caused by the effects of the low-pass characteristics of power amplifier. Chen et al. [8] developed another solution to the same problem using a double-loop compensation design based on AMBs. The first circuit used a notch filter to measure the unbalanced characteristic displacement signal of the rotor system. The second circuit was then a simple feedback loop for low speeds, which was replaced at high speeds by an adaptive circuit to adjust the control current to suppress the influence of the low pass characteristics of the power amplifier at high speeds. Zhang et al. [9] designed an AMB controller for a turbo molecular pump using other methods to suppress different kinds of vibrations. Shelke [10] controlled the four poles of a pair of active magnetic bearings based on the radial forces predicted by a two axes model and the response of a PID controller.

Besides control strategies, other researchers have focused on the structural design of the AMB itself. Filatov and Hawkins [11] studied the vibration reduction effects of various composite structures of AMBs for a 300 kW turbo compressor running at 40,000 rpm. Thye used a heteropolar electrically-biased radial actuator with a conventional electrically-biased

axial actuator, a heteropolar electrically-biased radial actuator with an electrically-biased axial actuator with a low target OD and a 'Side-By-Side' homopolar permanent-magnet-biased combination axial/radial actuator. They concluded that, for the prototype compressor, the third bearing had good performance, but its development was limited by the price and technology. Wen [12] studied the structural parameters of thrust magnetic bearings and radial magnetic suspension bearings. He established a model to optimize radial magnetic bearings and a finite element analysis to find the dynamic characteristics of magnetic bearings to optimize the design. Zhu and Zheng [13] established a 3D FEM model of magnetic bearings in ANSYS which included nonlinear material properties and rotor imbalances to design magnetic bearings.

Most previous research has concentrated on control methods for AMBs or the bearing structure to reduce the vibrations. However, the mechanical characteristics of the bearing and the whole structure are also important for vibration isolation since they are the main vibration transfer path.

This study focuses on the mechanical structural characteristics of the bearing and presents a finite element model of a 30 kW pump suspended on 5-DOF AMBs to investigate the effects of several key structural parameters on the magnetic pump vibrations. An optimized design is given with the corresponding mode shape as well as the seat vibration response calculated by the FE simulations. The result show that the modal frequency can be avoided and the acceleration response of the seat vibrations can be reduced by approximately 4 dB.

## II. DYNAMIC MODEL

### *A. Model estabilshment*

The pump chosen for this project was a magnetically suspended pump used for ship power equipment. The pump was installed vertically through four mattresses at the corners of the flange. The designed head was 50 m and the rated power was 30 kW. The pump included an independent motor and the water pump. The original bearing chamber was modified to replace the traditional bearings with magnetic levitation bearings. More details about the prototype pump are listed in TABLE I~~TABLE I~~ and shown in Figure 1~~Figure 1~~. Although the AMBs reduce the vibrations, this pump was not designed for the AMBs, so there is still room for further vibration reduction.

TABLE I PUMP DESCRIPTION

| | |
|---|---|
| Design head | 50 m |
| Rotational speed | 3000 rpm |
| Rated power | 30 kW |
| Blade number | 6 |
| Rotor weight | 75 kg |
| Type of cushion | BE-120 |
| Pump impeller type | Single stage centrifugal pump |
| Motor type | Three-phase asynchronous motor |

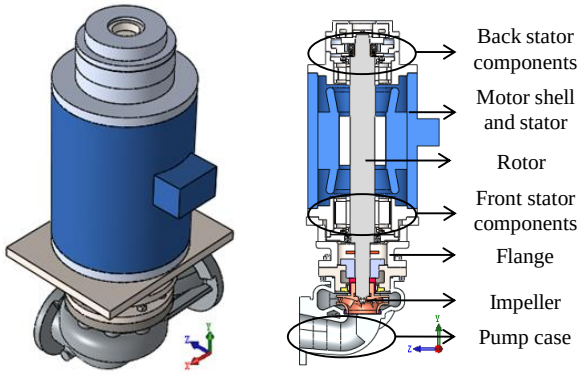


Figure 1 Magnetically suspended pump

The ANSYS model is shown in Figure 2. The model contains 27014 solid elements, 67 beam elements, and 4 integrated mass elements. The rotor is meshed by beam elements. The junction box as well as the pump shell are simplified to integrated mass points. The AMBs are simplified to spring-dampers with equivalent stiffnesses and with the damping related to the rotational speed. The cushion is replaced by three spring-dampers in different directions. All the components and the entire model have passed the grid independence validation. More details of the model are given in TABLE II.

TABLE II MODEL PARAMETERS

| Component | Element type | Number |
|---|---|---|
| Rotor | Beam188 | 66 |
| Impeller | Mass21 | 1 |
| Motor shell and stator | Solid186 | 4900 |
| Front stator components | Solid186, Targe170, Conta174 | 9332 |
| Back stator components | Solid186, Targe170, Conta174 | 14518 |
| Flange | Solid186 | 7632 |
| Pump case | Mass21, Solid186 | 2852 |
| AMBs | Combin14 | 80 |
| Cushions | Combin14 | 16 |
| Connections | Targe170, Conta174 | 1550 |
| Others | Solid186 | 768 |
| Total | / | 41716 |

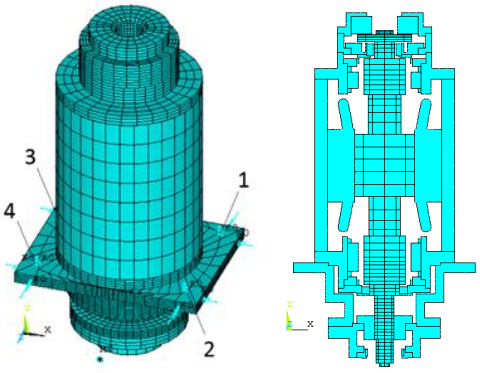


Figure 2 Magnetically suspended pump model

Two external excitations were analyzed with an unbalanced centrifugal force acting on the rotor and the hydrodynamic force acting on the impeller. The unbalanced force was based on the ISO 1940 guidelines for a dynamic balancing precision of G6.3. The hydrodynamic force was simplified to a time dependent force obtained from a CFD model that was assumed to not be affected by the system parameter changes. The frequency of the unbalanced force was 50 Hz and the main frequencies of the hydrodynamic force were 350 Hz and 700 Hz, which are equal to the unbalanced force frequency multiplied by the number of blades.

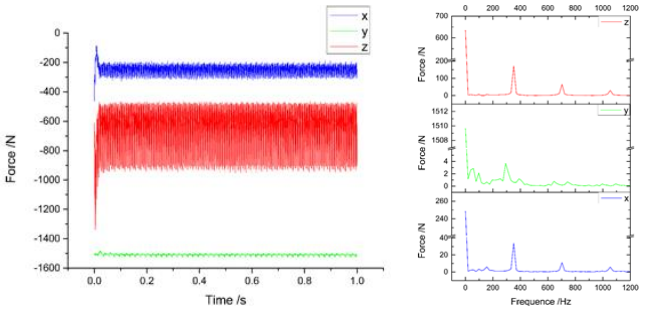


Figure 3 Hydrodynamic force

*B. Dynamic analysis*

**Modal analysis**

The first modal frequency is 4.976 Hz which is close to the experimental result of 5 Hz. The pump can be modeled as a rigid body to get the analytical solution for the first six modal frequencies. The calculation error was less than 5% as shown in TABLE III.

TABLE III ANALYTICAL AND NUMERICAL SOLUTIONS

| Mode description | Analytical solution (Hz) | Numerical solution (Hz) | Error (%) |
|---|---|---|---|
| Pump oscillating around x axis | 4.8429 | 4.9803 | 2.76 |
| Pump oscillating around z axis | 6.8205 | 6.9176 | 1.40 |
| Pump translating on the z axis | 11.4342 | 11.0812 | 3.19 |
| Pump translating on the y axis | 11.4382 | 11.3257 | 0.99 |
| Pump translating on the x axis | 19.2622 | 18.4397 | 4.46 |
| Pump rotating around y axis | 24.4487 | 23.7146 | 3.00 |

The modal analysis of the pump showed that the modes which might be excited by external forces are the rigid modes of the rotor and the first and second bending modes of the rotor.

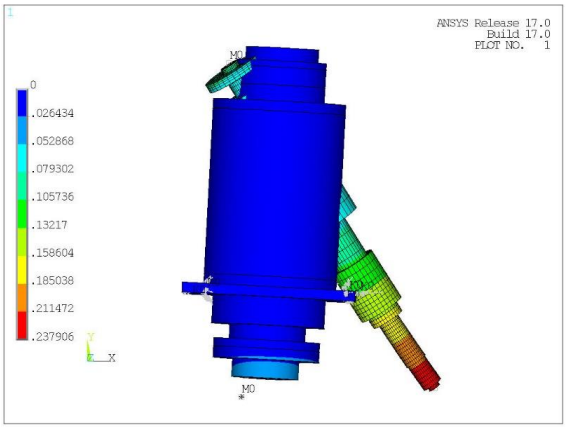


a) Rotor oscillating around the x or z axes

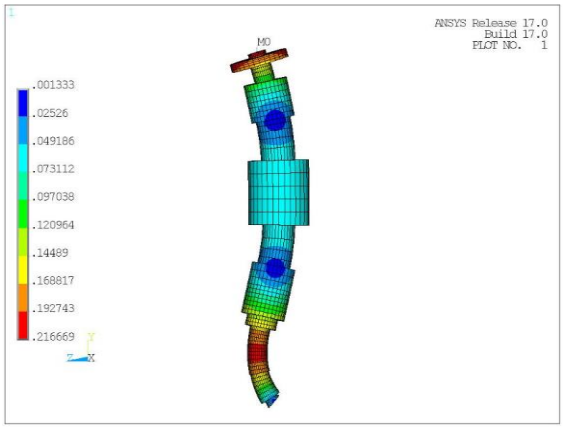


b) First bending mode of the rotor

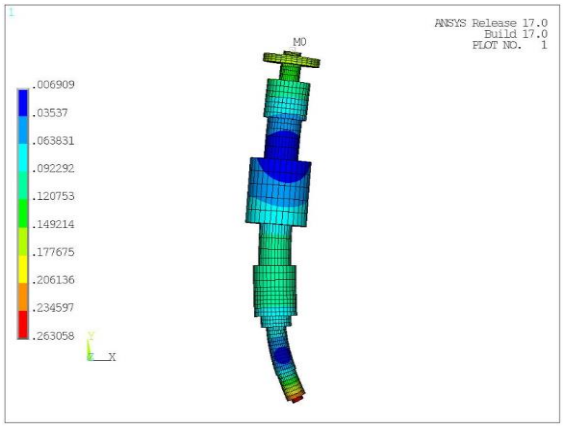


c) Second bending mode of the rotor

Figure 4 Modes that may cause resonance

Table IV PUMP VIBRATION MODES

| Number | 0 rpm (Hz) | 3000 rpm (Hz) | Mode description |
|---|---|---|---|
| 1 | 0.000209 | / | Free mode, rotor rotating around |
| 2 | 4.980 | 4.976 | Pump oscillating around x axis |
| 3 | 6.918 | 6.923 | Pump oscillating around z axis |
| 4 | 11.081 | 11.082 | Pump translating on the z axis |
| 5 | 11.326 | 11.326 | Pump translating on the y axis |
| 6 | 18.440 | 18.440 | Pump translating on the x axis |
| 7 | 23.715 | 23.715 | Pump rotating around y axis |
| 8 | 47.270 | 46.943 | Rotor oscillating around x axis |
| 9 | 47.865 | 48.185 | Rotor oscillating around z axis |
| 10 | 61.285 | 61.207 | Rotor oscillating around x axis |
| 11 | 62.017 | 62.123 | Rotor oscillating around z axis |
| 12 | 75.088 | 75.088 | Rotor translating on the y axis |
| 13 | 335.333 | 330.367 | First bending mode of the rotor |
| 14 | 335.333 | 340.210 | First bending mode of the rotor |
| 15 | 501.891 | 501.891 | First torsion mode of the rotor |
| 16 | 570.296 | 570.296 | First bending mode of the pump |
| 17 | 616.835 | 616.835 | First bending mode of the pump |
| 18 | 737.658 | 721.326 | Second bending mode of the |
| 19 | 737.658 | 754.740 | Second bending mode of the |
| 20 | 1046.607 | 1046.607 | Complex mode of the pump |

## Transient analysis

The response of the pump foot is shown in Figure 6~~Figure~~ 5 and Figure 6. The response consists of the free vibrations that decay over time because of the damping of the cushion and the forced vibrations induced by the periodic excitation force, which will not change over time. This study focuses on the second type.

The FFT transforms in Figure 7 show that from 0 to 0.1 s, the excitation force in the x direction excited horizontal vibrations of the pump with a frequency of 20 Hz in the x direction. The excitation force in the y direction excited horizontal translation of the pump at low frequencies of 5 Hz, 7 Hz and 11 Hz. The corresponding vibration mode is the pump oscillation mode in the x and z directions as well as the translation motion in the y direction. The excitation force in the z direction excited the horizontal vibration mode of the pump in the z direction with a frequency of 11 Hz. These excited vibrations were caused by the sudden application of the excitation force which decayed over time. The damping time was about 0.8 s, which means the calculations for the first 0.8 s are not important. By 0.8 s, these free vibration responses had almost disappeared. However, at this time, the 50 Hz vibrations still existed due to the frequency components of the hydrodynamic and unbalanced forces.

The hydrodynamic force had high-frequency components (350 Hz and 700 Hz), but the displacement responses were too small to observe. The effects of the high frequency components can more easily be seen in the acceleration response of the foot vibrations rather than the displacement response. However, this model is not able to predict the accelerations because the model contains too many nonlinear elements and the acceleration is hard to calculate.

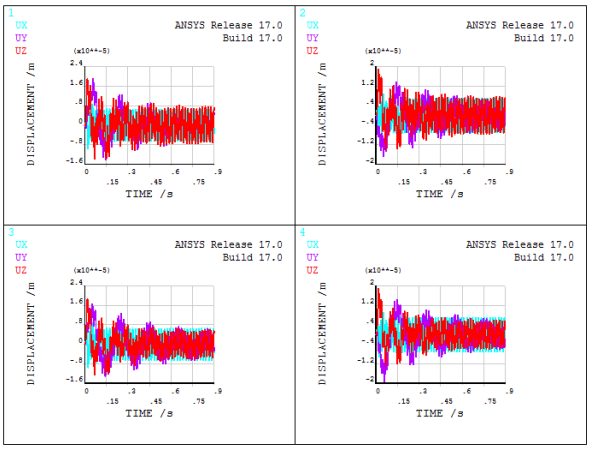


Figure 5 Vibration response of the foot during the transient state

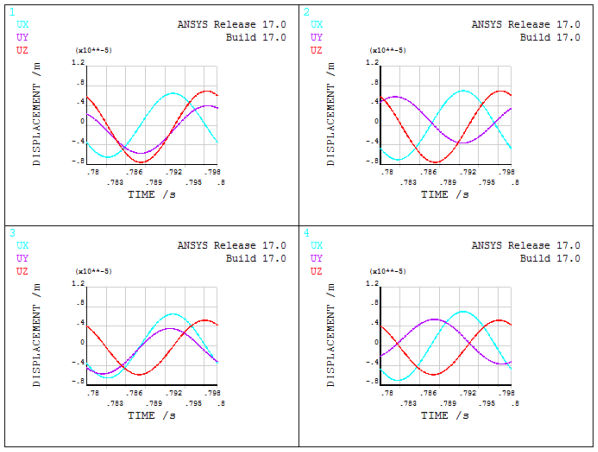


Figure 6 Vibration response on foot at steady state

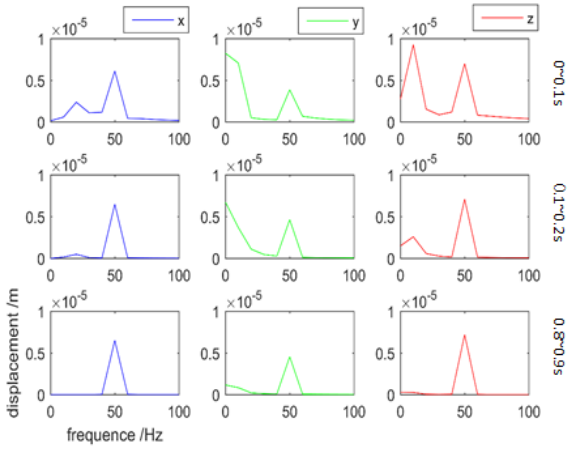


Figure 7 FFT transforms of the vibration response

### *C. Model simplification*

The previous section shows that the model can be simplified by reducing the decay time of the external excitation and by using multi-body dynamics to reduce the number of nonlinear elements to reduce the computational cost.

Figure 2 shows that the changes in the hydrodynamics force over time are quite complex. However, the forces can be approximated as the superposition of several small sinusoidal forces on top of constant forces in the three directions. The steady state vibration response is then a small vibration around the equilibrium position. The constant force only affects the equilibrium position of the system which was neglected to reduce the computational time the equilibrium position has little influence on the vibration response. The small sinusoidal forces were then directly applied to the system. The results are shown in TABLE V.

TABLE V VIBRATION DISPLACEMENTS OF THE FOOT BEFORE AND AFTER SIMPLIFICATION

| | X direction | | | Y direction | | | Z direction | | |
|---|---|---|---|---|---|---|---|---|---|
| | Before (dB) | After (dB) | Error (%) | Before (dB) | After (dB) | Error (%) | Before (dB) | After (dB) | Error (%) |
| **1** | 133.8 | 133.2 | 0.40 | 130.3 | 129.8 | 0.38 | 135.2 | 134.1 | 0.82 |
| **2** | 134.4 | 133.9 | 0.35 | 129.9 | 129.4 | 0.41 | 135.2 | 134.1 | 0.82 |
| **3** | 133.8 | 133.2 | 0.40 | 130.5 | 129.2 | 1.01 | 132.8 | 131.7 | 0.84 |
| **4** | 134.4 | 133.9 | 0.35 | 129.4 | 129.2 | 0.15 | 132.8 | 131.7 | 0.84 |

The model was then further simplified to further reduce the computational time and to obtain the acceleration response of the foot to be able to study the factors influencing the magnetically suspended pump vibrations.

These additional simplifications treated the back stator components, front stator components, motor stator, flange and pump case as rigid bodies. The rotor-bearing system and the motor shell were modeled as flexible bodies, with the motor shell stimulated by shell elements. This significantly reduced the system degrees of freedom, as shown in TABLE VI, which reduced the calculational time.

TABLE VI COMPARISON OF THE ORIGINAL AND SIMPLIFIED MODELS

| | Number of Elements | Number of Nodes |
|---|---|---|
| Before simplification | 41716 | 145320 |
| After simplification | 1156 | 7942 |

The accuracy of the simplified model was evaluated by comparing the displacements predicted by the original and simplified models for the modal analysis and the transient dynamic analysis in TABLE VII and TABLE VIII.

TABLE VII COMPARISON OF THE VIBRATION DISPLACEMENTS PREDICTED BY THE ORIGINAL AND SIMPLIFIED MODELS

| direction | Before simplification (dB) | After simplification (dB) | Error (%) |
|---|---|---|---|
| x | 133.242 | 136.565 | 2.433 |
| y | 129.810 | 127.238 | 2.021 |
| z | 134.065 | 136.667 | 1.904 |

TABLE VIII COMPARISON OF THE MODAL FREQUENCIES PREDICTED BY THE ORIGINAL AND SIMPLIFIED MODELS

| Number | Before simplification (dB) | After simplification (dB) | Error (%) |
|---|---|---|---|
| 1 | 0.000209 | 0.000198 | / |
| 2 | 4.980 | 4.9882 | 1.64 |
| 3 | 6.918 | 6.798 | 1.77 |
| 4 | 11.081 | 10.896 | 1.70 |
| 5 | 11.326 | 11.518 | 1.67 |
| 6 | 18.440 | 18.146 | 1.62 |
| 7 | 23.715 | 24.580 | 3.24 |
| 8 | 47.270 | 49.232 | 3.99 |
| 9 | 47.865 | 49.621 | 3.54 |
| 10 | 61.285 | 62.911 | 2.58 |
| 11 | 62.017 | 63.238 | 1.93 |
| 12 | 75.09 | 75.741 | 0.82 |
| 13 | 335.33 | 335.36 | 0.01 |
| 14 | 335.33 | 335.36 | 0.01 |
| 15 | 501.89 | 501.89 | 0.00 |
| 16 | 570.30 | / | / |
| 17 | 616.84 | / | / |
| 18 | 737.66 | 737.66 | 0.00 |
| 19 | 737.66 | 737.66 | 0.00 |
| 20 | 1046.6 | 1043.9 | 0.26 |
| 21 | 1076.2 | / | / |
| 22 | 1079.6 | 1079.6 | 0.00 |
| 23 | 1079.6 | 1079.6 | 0.00 |

TABLE VIII compares the same modes for the first 20 vibration modes. Since vibration modes 16, 17 and 21 disappeared, the number was extended to 23. The maximum difference between the predicted modal frequencies for the first 20 vibration modes is less than 4% for the mode of the rotor oscillating around the x or z axes. This is because the simplified model makes the pump more rigid which increases the system stiffness and boundary conditions. The transient dynamic analysis results are compared in TABLE VII where the response error is less than 2.5%, indicating that the simplification has no obvious effects on the system response. These results also indicate that the deformations of the front and back stator components and the flange are small and do not affect the results.

The simplified model was then used to calculate the acceleration response of the foot with the results shown in TABLE IX.

TABLE IX VIBRATION ACCELERATION OF THE FOOT PREDICTED BY THE SIMPLIFIED MODEL

| Measurement point | X direction (dB) | Y direction (dB) | Z direction (dB) |
|---|---|---|---|
| 1 | 115.9989 | 108.5395 | 116.1497 |
| 2 | 116.2626 | 110.0596 | 116.1497 |
| 3 | 115.9989 | 110.3298 | 116.3247 |
| 4 | 116.2626 | 107.0780 | 116.3247 |

## III. FACTORS INFLUENCING THE VIBRATIONS

### A. Vibration path

The vibration transmission path factors influencing the pump vibrations were analyzed to reduce the pump vibrations.

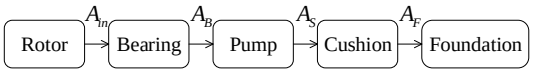


Figure 8 Vibration transmission path 1

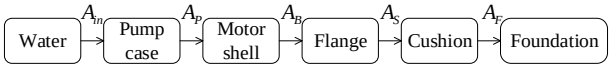


Figure 9 Vibration transmission path 2

The hydrodynamic and unbalanced forces are both transferred to the pump foot through the rotor, as shown in Figure 8. The hydrodynamic forces also have another transmission path to the base through the pump housing, as shown in Figure 9. However, the second transmission path is a complicated fluid-solid coupling problem, which is beyond the scope of this paper. Thus, this article only considers the first path.

The vibration transmission path factors influencing the magnetic pump vibrations include the rotor-bearing system, the pump body and the cushions. Since the rotor size is difficult to change, this article only studies the influence of the bearing stiffness in the rotor-bearing system, the mass distribution in the pump body and the effect of the model and the installation for the cushion.

### B. Factors influencing the vibrations

**Influence of bearing stiffness**

The influence of the front bearing stiffness the pump vibration modes is only reflected in the third and fifth modes for the horizontal translation modes of the pump in the two radial directions as shown in Figure 10 a. The modal frequencies gradually increase with increasing stiffness of the front bearing due to the low bearing stiffness. When the pump moves in the x or z directions, there is a slight relative vibration between the rotor and the rest of the pump. As the bearing stiffness increases, the overall stiffness increases up to a limit after which the rotor is essentially clamped and further increases of the bearing stiffness will not affect the overall stiffness.

The modal frequency of the oscillation mode swinging around the rear bearing increases with increasing of the front bearing stiffness as shown in Figure 10 b. When the front bearing stiffness exceeds $10^7$ N/m, the "rotor oscillation mode" is no longer just the rotor bearing-system mode but the rotor vibration vibrates the entire pump body. In addition, the first bending modal frequency of the rotor increases with increasing bearing stiffness after $10^7$ N/m.

In Figure 10 c, the radial foot response has a strong peak at $4\times10^6$ N/m and $5\times10^7$ N/m. At $4\times10^6$ N/m, the modal frequencies of rotor oscillating around the rear bearing are 49.936 Hz and 50.628 Hz, and the unbalanced force will cause resonance. At $5\times10^7$ N/m, the first bending modal frequencies of the rotor are 345.993 Hz and 355.604 Hz, and the hydrodynamic force will cause resonance. The axial foot vibration also changed with the radial bearing stiffness. Since the vibrations also contained radial oscillating component which influenced the axial vibration response of the foot, the change in the radial bearing stiffness influenced the oscillating vibration modes.

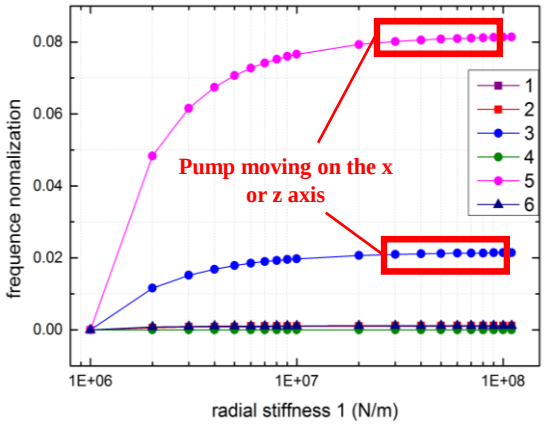


a) Influence on the pump modes

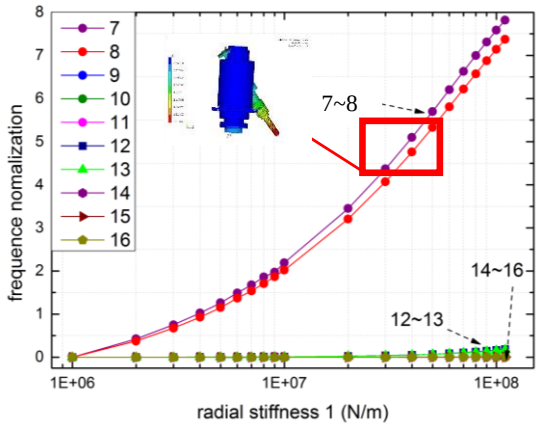


b) Influence on the rotor modes

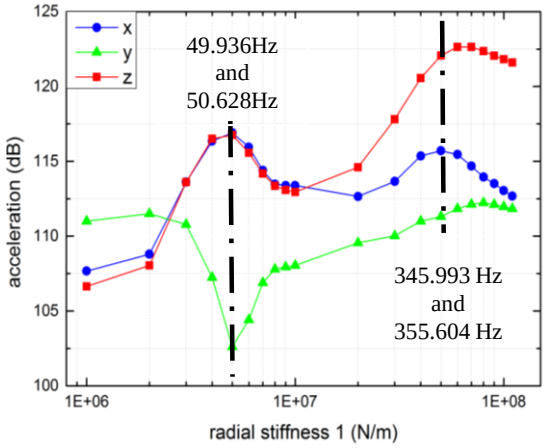


c) Influence on the response

Figure 10 Influence of the front bearing stiffness

The influence of the rear bearing stiffness on the vibration is similar to that of the front bearing, as shown in Figure 11. In fact, in Figure 11 c, the modal frequency of the rotor oscillation mode around the front bearing is always around 50 Hz, so the vibration response is relatively large.

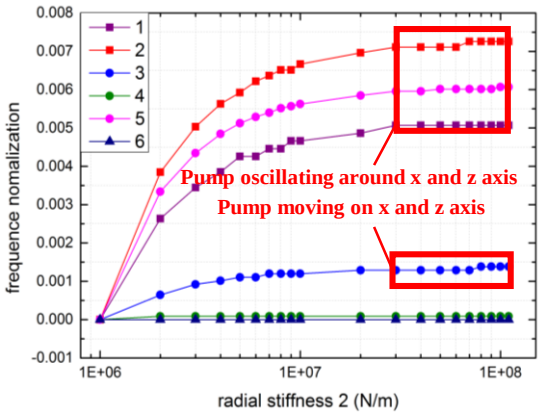


a) Influence on the pump modes

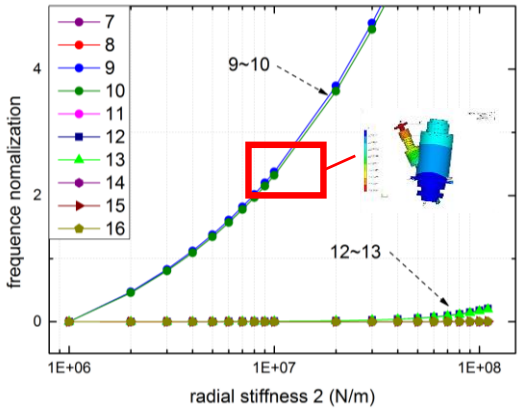


b) Influence on the rotor modes

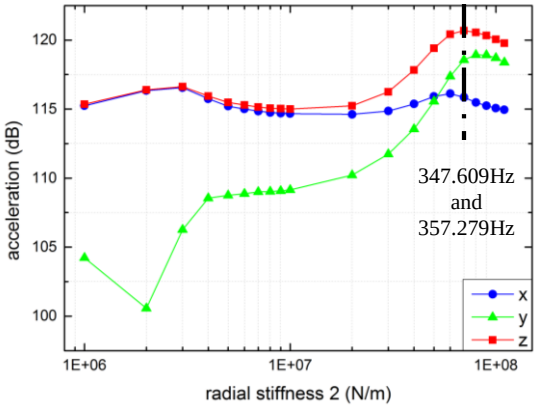


c) Influence on the response

Figure 11 Influence of the rear bearing stiffness

The results also show that an increase of the axial bearing stiffness only affects the modal frequency of the rotor axial vibration and has little influence on the vibration response.

**Influence of the mass distribution**

In terms of the modal frequencies, the masses of the front and back stator components strongly affect the oscillation modes and the pump translation modes, that is, the top six modes in the system. The front stator mass changes the three translation modal frequencies while the back stator mass changes the two oscillation modal frequencies as well as the translation modal frequencies on the y axis. The horizontal "translational vibration" of the whole pump is not absolutely translational motion, but has oscillations rotating the center away from the pump itself. Thus, the front and rear component masses have similar, symmetric effects on the modal frequencies.

The front and back stator component masses have different effects on the foot response. Increasing the front component mass reduces the radial response of the foot and increases the axial response. In contrast, increasing the back component mass does not affect the radial response of the foot but reduces the axial response.

In addition, the simulations show that the motor shell thickness has little influence on the modal frequencies and the foot vibration. The junction box position, even though makes the motor shell not symmetric, does not greatly affect the pump vibrations due to its small weight (3.75 kg).

Therefore, for vertically installed pumps, the masses at the top and bottom greatly influence the vibrations, while the mass in the middle has relatively little influence. Thus, a vertical pump can be approximately regarded as an inverted pendulum.

TABLE X INFLUENCE OF MASS INCREASES ON THE MODAL FREQUENCIES

| | Mode description | Motor shell thickness | Front stator component mass | Back stator component mass |
|---|---|---|---|---|
| 1 | Pump oscillating around x axis | — | — | ↓ |
| 2 | Pump oscillating around z axis | — | — | ↓ |
| 3 | Pump translating on the z axis | — | ↓ | — |
| 4 | Pump translating on the y axis | — | ↓ | ↓ |
| 5 | Pump translating on the x axis | — | ↓ | — |
| 6 | Pump rotating around y axis | — | — | — |

TABLE XI INFLUENCE OF MASS INCREASES ON THE FOOT RESPONSE

| direction | Motor shell thickness | Front stator component mass | Back stator component mass |
|---|---|---|---|
| x | — | ↓ | — |
| y | — | ↓ | — |
| z | — | ↑ | ↓ |

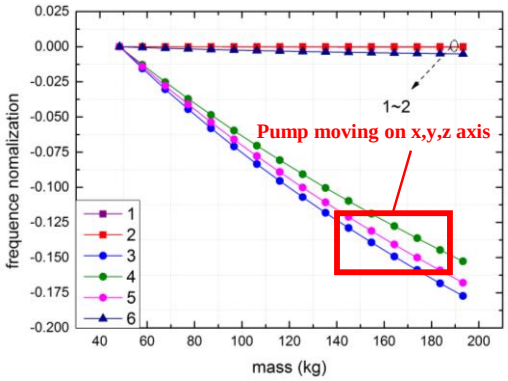


a) Influence on the pump modes

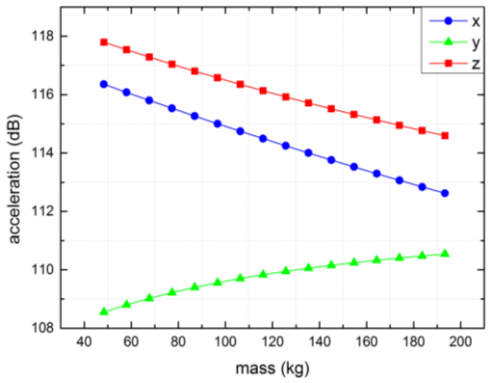


b) Influence on the response

Figure 12 Influence of the front stator component mass

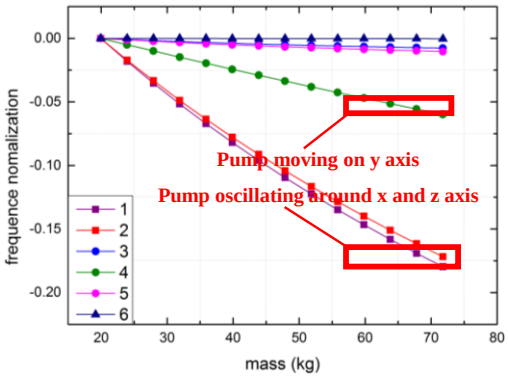


a) Influence on the pump modes

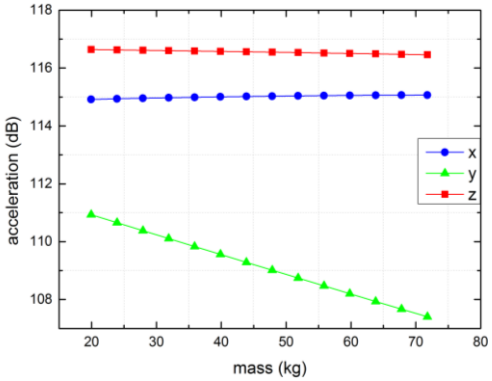


b) Influence on the response

Figure 13 Influence of back stator component mass

**Influence of the cushion model and installation direction**

The prototype used the BE-120 cushion mode positioned in the x, y and z direction as shown in Figure 1~~Figure 1~~ and Figure 2~~Figure 2~~. The x and z directions could be exchanged during installation. Increases of the cushion model number indicate increasing stiffness. The abscissa in Figure 14 is the cushion model number.

Figure 14 a shows the variation of the modal frequencies with the cushion model installed in the original direction. If the installation in the two radial directions are reversed, there is no significant difference. The cushion stiffness only affects the modal frequency of the top six vibration modes of the pump and does not affect the modal frequencies of the rotor.

The coordinate directions without the subscripts in Figure 14 b indicate when the cushions are installed in the original direction, while the subscript 1 indicates the installation with the x and z directions reversed. With the original installation direction, the radial vibration in the orthogonal direction differ some with this difference decreasing with increasing cushion stiffness, while the axial vibrations increase. When the x and z directions are reversed, there is little difference in the radial orthogonal vibrations. With increasing cushion stiffness, the radial vibrations are almost unchanged while the axial vibrations are greatly reduced. In fact, if the installation only focuses on the axial response of the foot, the installation direction of the cushion should be reversed.

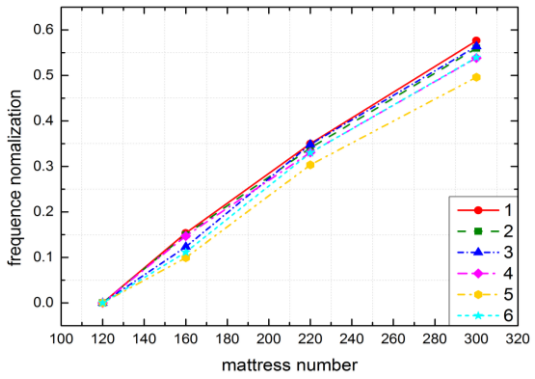


a) Influence on the pump modes

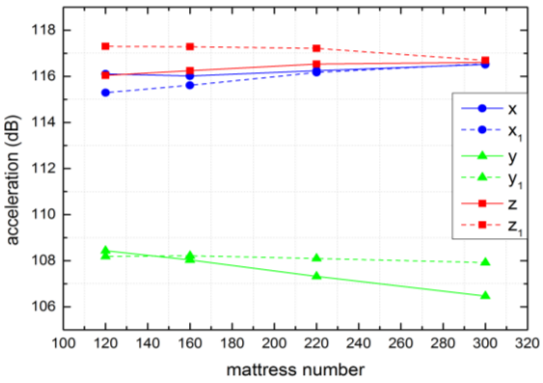


b) Influence on the response

Figure 14 Influence of the cushion model and installation direction

Changing the pump mounting to a side-fixed support will significantly change the modal frequency because the

mounting affects the pump vibration modes but only the top six modes. However, changing the support position will not solve the resonance problem in the prototype.

## IV. OPTIMIZED DESIGN

The mechanical design of the front and rear stator components of the magnetic pump has already been completed and cannot be easily changed. Therefore, changes in the front and rear end component masses was not considered in the optimization process. The magnetic bearing stiffness is controlled by the controller parameters (such as the proportion, integral and differential control parameters in the PID controller) from $10^6$-$10^8$ N/m, which is a very wide range. This is also one of the advantages of magnetic bearings. The findings given here on the effects of the various factors on the vibrations was combined with engineering practice to determine a good set of design parameters to reduce the pump vibrations. The optimal and original parameters are listed in TABLE XII.

TABLE XII OPTIMAL AND ORIGINAL DESIGN PARAMETERS

| | Optimal design | Original design |
|---|---|---|
| Front bearing stiffness (N/m) | $1\times10^7$ | $3.765\times10^6$ |
| Rear bearing stiffness (N/m) | $1\times10^7$ | $3.765\times10^6$ |
| Axial bearing stiffness (N/m) | $3\times10^7$ | $1.443\times10^6$ |

The modal frequencies of the improved design for the dangerous vibration modes (the red numbers in

Table IV~~Table IV~~) avoid rotor oscillation modal frequencies near 50 Hz. After the redesign, the foot vibration of the magnetic suspension pump was reduced by about 4 dB. The results in Table XIII show that the new design does not avoid the first and second rotor bending modal frequencies around 350 Hz and 700 Hz. The G6.3 Unbalanced Precision Standard indicates that the foot response mainly depends on the unbalanced force. Therefore, this design should focus on avoiding the rotor oscillation modal frequencies around 50 Hz. Additionally, the flexible mode frequencies of the rotor are difficult to change by just altering the bearing stiffness and the cushion design. The best choice is to redesign the shaft segment or change the bearing support positions.

TABLE XIII COMPARISON OF THE MODAL FREQUENCIES FOR THE OPTIMAL AND ORIGINAL DESIGNS

| Number of mode | Optimal design (Hz) | Avoidance ratio (%) | Original design (Hz) | Avoidance ratio (%) |
|---|---|---|---|---|
| 7 | 76.734 | 53.468 | 49.232 | 1.536 |
| 8 | 77.410 | 54.820 | 49.621 | 0.758 |
| 12 | 331.695 | 5.230 | 335.36 | 4.183 |
| 13 | 341.531 | 2.420 | 335.36 | 4.183 |
| 15 | 720.216 | 2.888 | 737.66 | 5.380 |
| 16 | 753.641 | 7.663 | 737.66 | 5.380 |

TABLE XIV COMPARISON OF THE ACCELERATION RESPONSES OF THE OPTIMAL AND ORIGINAL DESIGNS

| direction | Optimal design (dB) | Original design (dB) |
|---|---|---|
| x | 111.7547 | 115.9989 |
| y | 106.7904 | 108.5395 |
| z | 111.2848 | 116.1497 |

## REFERENCES


[1] Yang J.G.. “Multiplicity analysis of friction fault characteristics of rotating machinery”, Electrical Equipment 8.10 (2007): 1-4. (in Chinese)

[2] Kasarda, M. "An overview of active magnetic bearing technology and applications." Shock and Vibration Digest, 2000 32 (2000): 91-99.

[3] Zheng S, Chen Q, Ren H. "Active balancing control of AMB-rotor systems using a phase-shift notch filter connected in parallel mode." IEEE Transactions on Industrial Electronics 63.6 (2016): 3777-3785.

[4] Dai X Z, Zhang X H, Liu G H. "Decouping Control of Induction Motor Based on Neural Networks Inverse." Proceedings of the Csee 24.1 (2004): 112-117..

[5] Schweitzer, Gerhard, Hannes Bleuler, and Alfons Traxler. "Active magnetic bearings, basics, properties and application of active magnetic bearings." vdf, Hochschulverlag an der ETH Zürich, Zürich, Switzerland (1994).

[6] Tanaka N, Uchiyama N, Watanabe T "Levitation and vibration control of a flexible rotor by using active magnetic bearing." Journal of System Design and Dynamics 3.4 (2009): 551-562.

[7] Zheng, S.Q., Feng, R.. “Feedforward compensation control of rotor imbalance for high-speed magnetically suspended centrifugal compressors using a novel adaptive notch filter”, *Journal of Sound and Vibration*, 336, pp. 1-14, 2016.

[8] Chen Q, Liu G, Zheng S, “Suppression of imbalance vibration for AMBs controlled driveline system using double-loop structure”, *Journal of Sound and Vibration* ,337,pp.1–13,2015

[9] Zhang, K, Dong J, Dai X, Zhang X., "Vibration Control of a Turbo Molecular Pump Suspended by Active Magnetic Bearings." ASME 2011 Turbo Expo: Turbine Technical Conference and Exposition. American Society of Mechanical Engineers, 2011

[10] Shelke, S.. "Controllability of Radial Magnetic Bearing." Procedia Technology 23 (2016): 106-113.

[11] Filatov, A., and Hawkins, L. "Comparative study of axial/radial magnetic bearing arrangements for turbocompressor applications." Proceedings of the Institution of Mechanical Engineers, Part I: Journal of Systems and Control Engineering 230.4 (2016): 300-310.

[12] Wen, Y.S. The research of the magnetic properties of magnetic suspension bearing in fan and bearing capacity analysis. MS thesis. University of Science and Technology Liaoning, 2015.(in Chinese)

[13] Zhu, C. S., and J. Q. Zheng. "Analysis on Electromangentic Bearing Characteristics Based on ANSYS." Bearing (2004).